Received Date: March 2025 Revised: April 2025 Accepted: June 2025

Study the differential cross-section of scattering by using Gaussian potential in presence of laser

Santosh Kumar Das, Saddam Husain Dhobi

Corresponding Authors: saddam@ran.edu.np/dassantosh29@gmail.com

Doi: *https://doi.org/10.3126/ppj.v5i1.85843*

Abstract

The study of electron–atom scattering provides fundamental insights into particle interactions and quantum dynamics. The differential cross-section (DCS) is a key quantity that quantifies the probability of scattering at specific angles and energies. Modeling the target potential accurately is essential for precise predictions, and the Gaussian potential offers a smooth and well-defined representation of atomic fields. When combined with external laser fields, the scattering behavior becomes more complex, as the laser modifies the interaction dynamics and introduces polarization-dependent effects. The aim of this work is understood how polarization type, scattering angle, momentum, photon energy and distance separation effect the interaction of electron-atom in laser field. For this study, a theoretical model was developed using Volkov wavefunctions, Gaussian potentials, the S-matrix formalism, and Bessel functions within the framework of the Kroll–Watson approximation. The resulting model was implemented in MATLAB to analyze and compare the behavior of the newly derived equations. The observations show, elliptical polarization produces the highest DCS, followed by circular and linear polarizations, and that zero-order Bessel functions yield higher magnitudes than first-order. Equilibrium occurs when electrostatic interaction energy equals particle rest energy, with resonance phenomena observed around specific energies and momentum transfers. Limitations include the challenge of experimentally measuring DCS for higher-order Bessel functions due to reduced magnitudes. Future work is recommended to extend the study to multi-photon and higher-order interactions and to explore experimental validation of theoretical predictions. Overall, the results provide insight into controlled scattering processes in laser-modulated fields.

Keywords: Electron–atom scattering, differential cross-section, Gaussian potential, external laser fields, polarization type

Introduction

This study investigates the DCS in the presence of a linearly polarized laser field using Bessel functions of various orders, with oxygen molecules as targets under the Lennard-Jones potential. The theoretical model reveals electron energy gain and loss in the presence of oxygen. A deep peak in the DCS indicates alignment between incident and final energies, suggesting possible new particle formation. A DCS minimum signifies strong electron-

target interaction, potentially forming particles smaller than both. The zero-order Bessel function shows a higher DCS compared to higher orders due to its distinct properties. At a zero-radian scattering angle, the DCS reaches a minimum, indicating increased particle interaction and formation, emphasizing the angle's significance in such processes (Shrestha et al., 2023). The laser-assisted scattering of an electron by an attractive one-dimensional δ-function potential, and solve analytically a coupled-channel Lippmann-Schwinger equation for the full scattering amplitude. Energy, in multiples of the laser frequency, can be absorbed or emitted by the electron during the scattering, and the corresponding superelastic and inelastic, as well as the elastic, scattering amplitudes are all determined exactly. Stimulated recombination resonances are observed in all channels (LaGattuta, 1994). We discuss various important aspects of the theory of multiphoton free–free transitions. First we show, in the simple framework of potential scattering, the necessity for a description of the laser field to take into account the actual experimental conditions such as beam focusing and pulsed and multimode operations. We then generalize the study to the collisions of fast electrons with atoms in intense laser fields and show how the dressing of the atomic states by the external radiation field can affect the scattering cross sections. Finally, we consider the role played by statistical fluctuations of the laser field. To this end, we develop the pre-Gaussian model of laser noise and show how this formalism can be included in the theory of multiphoton free–free transitions (Francken & Joachain ,1990).

A body of work has explored the interaction of an electron with a laser electric field while under a one-dimensional attractive δ-function potential. These studies typically involve numerical solutions of the time-dependent Schrödinger equation, focusing on photoionization rates across the strong-field regime (10^{9}–10^{14} W/cm^{2}), though not the ultrastrong-field domain ($\geq 10^{16}$ W/cm^{2}). Laser-modified scattering rates for this potential have not been addressed, but laser-assisted scattering has been studied in other systems. Recently, several studies have examined the stabilization of bound states against photoionization at high laser intensities for various potentials (LaGattuta, 1994). Much theory uses the Kroll-Watson approximation, treating laser interaction nonperturbatively in scattering. It ignores laser-atom interaction, simplifying the result: the laser-modified cross section is just the field-free one adjusted by laser-electron effects. In electron-atom scattering with low-frequency lasers, energy can change by photon multiples so-called free-free transitions (Wallbank & Holmes, 1993).

In intense laser fields, atoms emit high-energy electrons and high-order harmonics. This occurs as an electron is ionized, accelerated by the laser field, and then rescattered by its parent ion. The rescattering can lead to above-threshold ionization, harmonic generation, or further excitation/ionization of bound electrons (Kulander, 1995). Since the 1970s, laser-

assisted atomic collisions have been studied, with renewed interest due to recent experimental advances. Intense lasers can greatly enhance charge exchange in ion-atom collisions, especially under resonant conditions. Current work explores how lasers can significantly affect collision outcomes, with high-intensity pulsed lasers often required (Anis et al., 2006). Atoms in strong laser fields can emit high-energy electrons and photons, explained well by the quantum-orbit (path integral) formalism (Milošević et al., 2006). The invention of the laser in 1960 revolutionized physics research. Progress in shortening pulse duration and increasing intensity has enabled femtosecond and attosecond lasers, allowing precise studies of electron motion. Higher intensities help control fast processes, supporting the generation of ultrashort light pulses (Maiman, 1960; Mourou & Tajima, 2011; Krausz & Ivanov, 2009; Di Piazza et al., 2012).

Most theories of laser-assisted particle-atom collisions use the single-mode laser approximation, but real lasers have complex features like multimode operation and pulse shaping. These characteristics significantly affect light-matter interactions. To match experimental conditions, more accurate models—such as N-mode or chaotic field descriptions—are needed (Daniele & Ferrante, 1981). Correlated double ionization is a key topic in intense-field physics. Though one-photon-induced cases were known, multi-photon ionization was thought to involve only one active electron. This changed in 1992, when experiments on helium showed double ionization rates far exceeding sequential predictions, revealing strong electron correlation (Yudin & Ivanov, 2001). At high laser intensities, electron-photon scattering is dominated by ponderomotive effects. Electrons can gain or lose energy from laser pulses like "surfing" on light waves, as observed experimentally and explained by classical models (Bucksbaum et al., 1987). Laser microtechnology enables precise, cost-effective processing of micrometer-scale components in electronics and optics (Metev & Veiko, 2013).

Methods and materials

The time dependent Schrödinger equation can be used to describe the conduction-band electrons dynamics of the LCQWWs in the (x,y) plane: (Liu et al., 2009 ;Kurmi et al., 2025).

$$\left[\frac{1}{2m}\left(p-\frac{e}{c}A(t)\right)^2+V\right]\psi(x,y,t)=i\hbar\frac{\partial\psi(x,y,t)}{\partial t} \qquad (1)$$

We solve Schrodinger equation which depends on time to obtain the wave form of an electron connected to an external electromagnetic field. The laser field can be represented by the vector potential A(t) in the dipole approximation. Where V is potential which is Gaussian potential (Agrawal & Prakash, 2002).

$$V(r) = V_0 \exp\left[-\left(\frac{r}{R}\right)^2\right] \quad (2)$$

Consequently, an electron connected to an external field of electromagnetic radiation has the following Hamiltonian (Kim, 2022).

$$H_{e-laser} = \frac{1}{2m}[\hat{p} - eA(t)]^2 \quad (3)$$

where e = |e| denotes the elementary charge, m represents the electron mass, and p̂ represents the momentum of the operator. The state wave function $X(r,t)$ time-dependent Schrodinger equation (Kim, 2022) for atomic unit is thus

$$\frac{i\partial X(r,t)}{\partial t} = \frac{1}{2}\left[\left(\hat{p} - A(t)\right)^2 + V\right] X(r,t) \quad (4)$$

The Schrodinger equation's time-dependent wave function is (Maurer, & Keller ,2021).

$$X(r,t) = \frac{1}{(2\pi)^{3/2}} \exp\left\{i\frac{p}{\hbar}.\left(r + \frac{e}{m}\int A(t)\right) - i\frac{E}{\hbar}t - i\frac{e^2}{2m\hbar}\int A^2(t)\,(t)\right\}dt \quad (5)$$

Where, E is the kinetic energy of projected electron. This goes by the name of the Volkov wave function. Kinetic energy of free electron's is E. For elliptical polarization, we also have vector potential (Yadav et al., 2020)

$$A = a\left[\hat{x}\cos(\omega t) + \hat{y}\sin(\omega t)\tan\left(\frac{\eta}{2}\right)\right] \quad (6)$$

From equation (5) and (6), we get

$$X(r,t) = \frac{1}{(2\pi)^{\frac{3}{2}}} \exp\left\{i\frac{p}{\hbar}.\left(r + \frac{e}{m}\int a\left[\hat{x}\cos(\omega t) + \hat{y}\sin(\omega t)\tan\left(\frac{\eta}{2}\right)\right]dt\right) - i\frac{E}{\hbar}t - i\frac{e^2}{2m\hbar}\int a^2\left[\hat{x}\cos(\omega t) + \hat{y}\sin(\omega t)\tan\left(\frac{\eta}{2}\right)\right]^2 dt\right\} \quad (7)$$

After integrating the equation (7) both sides with respect to t. we get,

$$X(r,t) = \frac{1}{(2\pi)^{\frac{3}{2}}} \exp\left\{i\frac{p}{\hbar}.\left(r + \frac{e}{m}R\sin(\omega t - \gamma)\right) - i\frac{E}{\hbar}t - i\frac{e^2}{2m\hbar}\left[-\frac{a^2}{4\omega}\left\{\left[\tan^2\left(\frac{\eta}{2}\right) - 1\right]\sin(2\omega t) - 2\omega t\left[1 + \tan^2\left(\frac{\eta}{2}\right)\right] + 2\cos(2\omega t)\tan\left(\frac{\eta}{2}\right)\right\}\right]\right\} \quad (8)$$

For linear opalization $\eta = 0$, for elliptical polarization $\eta = \pm\pi$ and for $\eta = \frac{\pi}{2}$ in equation (8) using equation (8). S-matrix is a element of time development operator between unperturbed asymptotic in and out state when times tends to $-\infty\ to + \infty$ where as transition matrix in a fixed time. Due to the application of quantum scattering theory combined with a classical treatment of the electromagnetic field, the model is regarded as semiclassical. Equation is used in a derivation akin to that presented by (Kroll and Watson, 1973).

$$S_{fi} = \delta_{fi} - \frac{i}{\hbar}\int_{-\infty}^{+\infty}\left\langle X_f(r,t)\middle|V(r)\middle|X_i(r,t)\right\rangle dt \quad (9)$$

$$T_{fi} = \frac{i}{\hbar}\int_{-\infty}^{+\infty}\left\langle X_f(r,t)\middle|V(r)\middle|X_i(r,t)\right\rangle dt \quad (10)$$

Where, X_f and X_i *is* final and initial wave function of after and before scattering. To evaluate the matrix element

$$T_{fi} = \int_{-\infty}^{\infty} \langle \psi_f^E(r,t|V(r)|\psi_i^E(r,t) \rangle \; dt \qquad (11)$$

From equation (8) and (11), we get

$$T_{fi}$$
$$= \int d^3r \int_{-\infty}^{\infty} \left(\frac{1}{(2\pi)^{\frac{3}{2}}} \exp\left\{ -i\frac{p_f}{\hbar}.\left(r + \frac{e}{m} R\sin(\omega t - \gamma)\right) + i\frac{E_f}{\hbar}t \right.\right.$$
$$+ i\frac{e^2}{2m\hbar}\left[-\frac{a^2}{4\omega}\left\{ \left[\tan^2\left(\frac{\eta}{2}\right) - 1\right]\sin(2\omega t) - 2\omega t\left[1 + \tan^2\left(\frac{\eta}{2}\right)\right] \right.\right.$$
$$\left.\left.\left. + 2\cos(2\omega t)\tan\left(\frac{\eta}{2}\right)\right\}\right]\right\} \Big) |V(r)| \left(\frac{1}{(2\pi)^{\frac{3}{2}}} \exp\left\{ i\frac{p_i}{\hbar}.\left(r + \frac{e}{m} R\sin(\omega t - \gamma)\right) - i\frac{E_i}{\hbar}t \right.\right.$$
$$- i\frac{e^2}{2m\hbar}\left[-\frac{a^2}{4\omega}\left\{ \left[\tan^2\left(\frac{\eta}{2}\right) - 1\right]\sin(2\omega t) - 2\omega t\left[1 + \tan^2\left(\frac{\eta}{2}\right)\right] \right.\right.$$
$$\left.\left.\left. + 2\cos(2\omega t)\tan\left(\frac{\eta}{2}\right)\right\}\right]\right\} \Big) dt \qquad (12)$$

On substituting value of potential from above on equation (12) for spherical coordinate system with Bessel function we have

$$T_{fi}$$
$$= \frac{1}{(2\pi)^3} \int_{-\infty}^{\infty} \int_{o}^{2\pi} \int_{0}^{\pi} \left(\exp\left(iKr \right.\right.$$
$$\left.\left. - \left(\frac{r}{R}\right)^2 \right) \exp(-\gamma) \sum_{n=-\infty}^{\infty} J_n(K\alpha) \right) V_0 \; r^2 sin\theta \; d\theta \; d\phi \; dr \qquad (13)$$

Also, we have relation between differential cross-section and T-matrix(Kavazović et al., 2021).

$$\frac{d\sigma}{d\Omega} = \frac{K_f}{K_i} \left| T_{fi} \right|^2 \qquad (14)$$

Now solving the equation (13) and putting in equation (14) we get, DCS for zero order Bessel function as in atomic unit term as

$$\frac{d\sigma}{d\Omega} = \frac{k_f}{k_i}\left|-\frac{V_0\exp(-\gamma)}{(2\pi)^2 i\Delta p}\left\{\frac{\sqrt{\pi}}{4}(i\Delta p\cos\theta)\exp\left(\frac{(a\Delta p\cos\theta)^2}{4\omega^2}\right)\left(\frac{ia}{\omega}\right)^3 erf\left(\frac{\frac{-2r\omega^2}{a^2}-i\Delta p\cos\theta}{2\sqrt{i\Delta p\cos\theta}}\right)\right.\right.$$
$$\left.\left.+a^2\frac{\exp\left(r\left\{i\Delta p\cos\theta+\frac{r\omega^2}{a^2}\right\}\right)}{2\omega^2}\right\}\right|^2 \quad (15)$$

Also solving the equation (13) and putting in equations (14) we get, DCS for first order Bessel function as in atomic unit term as

$$\frac{d\sigma}{d\Omega} = \frac{k_f}{k_i}\left|-\frac{aV_0\exp(-\gamma)}{(2\pi)^2 2\omega}\left\{\frac{\sqrt{\pi}}{4}(i\Delta p\cos\theta)\exp\left(\frac{(a\Delta p\cos\theta)^2}{4\omega^2}\right)\left(\frac{ia}{\omega}\right)^3\right.\right.$$
$$\left.\left.+a^2\frac{\exp\left(r\left\{i\Delta p\cos\theta+\frac{r\omega^2}{a^2}\right\}\right)}{2\omega^2}\right\}\right|^2 \quad (16)$$

Results and discussion

DCS for zero order Bessel function

To analyze the behavior of the proposed equation (15), various parameter ranges were considered. The investigation covered incidence energies from 0 to 5 MeV, scattering angles between 0° and 60°, quantum dot sizes ranging from 0 to 10 Å, and laser-dressed parameters varying from 0 to 40 Å, as reported by Durak and Sakiroglu (2023). Figures 1(a)–1(c) illustrate how the DCS changes with scattering angle. In Figure 1(a), the DCS gradually decreases as the scattering angle increases, reaching its minimum value at approximately 75°. This trend resembles the amplitude decay pattern characteristic of Bessel functions. Physically, this implies that the probability of interaction between the projectile and the target diminishes with increasing scattering angle. By contrast, Figures 1(b) and 1(c) display an opposite trend, where the DCS increases with the scattering angle. In the elliptical and circular polarization cases, the variation pattern differs notably from the linear case. Specifically, for elliptical polarization, a sharp increase in DCS is observed beyond a scattering angle of 40°, whereas this steep rise is absent in the circular polarization case. Moreover, the presence of a minimum DCS corresponds to a threshold interaction region. Within this region, the interaction probability remains constant, and beyond it, the projectile

cannot approach the target any closer. Figure 1 (a) has similar nature that of Kurmi et al. (2025) shows that DCS decrease with scattering angle.

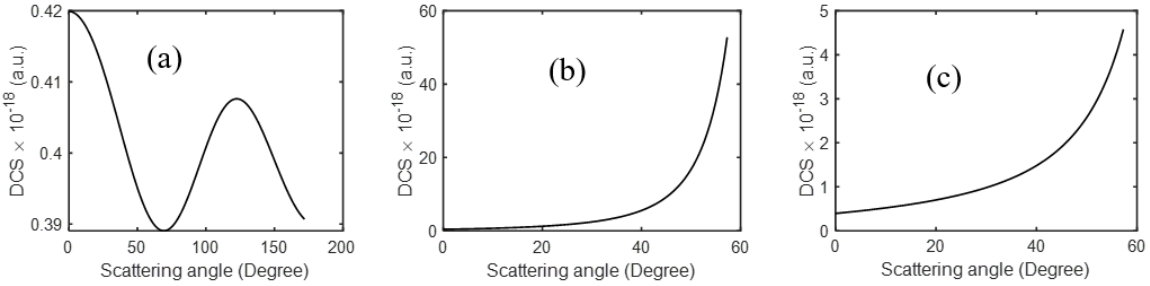

Figure 1: Dcs with scattering angle (a) linear, (b) elliptical, (c) circular of zero order bessel fucntion

The DCS in the elliptical polarization case is higher because elliptical polarization oscillations cover a broader interaction region due to their helicity characteristics. In contrast, circular polarization oscillations are more confined, with a fixed rotational pattern, resulting in a smaller interaction region than in the elliptical case. Linear polarization covers an even smaller interaction region compared to circular polarization, as depicted in Figure 1. This behavior is determined by the ellipticity, which depends on the oscillation pattern. The broader oscillation field in the elliptical case enhances the probability of interaction between the projectile and the target. As the oscillating field approaches the target, the likelihood of interaction increases because the polarization field modifies the projectile's motion, thereby increasing the resultant amplitude.

Figure 2 presents the DCS variation with momentum for the three polarization types—linear, elliptical, and circular. Observations indicate that the elliptical case consistently exhibits the highest DCS, followed by the circular case, with the linear case showing the lowest values. These measurements were taken at a scattering angle of 5°. Beyond approximately 0.5 eV, the DCS is higher; however, after this point, it decreases gradually and eventually levels off. The reduction in DCS with increasing projectile energy is attributed to the dominance of the projectile's kinetic energy over the target's field. Below 0.5 eV, the target's field dominates the interaction, but as the projectile energy increases, its ability to penetrate the target's field reduces the effective interaction region. Around 1 eV, the DCS becomes constant, indicating that the projectile and target particles have reached an equilibrium state in which the electrostatic interaction energy equals their rest energy. This equilibrium can be interpreted as a manifestation of the self-interaction of the particle within its own field. The DCS variation with momentum change shows a similar trend when compared to the results of Bohora et al. (2025) for electron–atom interactions in laser fields. Additionally, Dhobi et al. (2025) and Shrestha et al. (2024) studied the DCS as a function of

incidence energy and observed a damping-like decrease; however, their analysis considered thermal effects, which are not included in the present study.

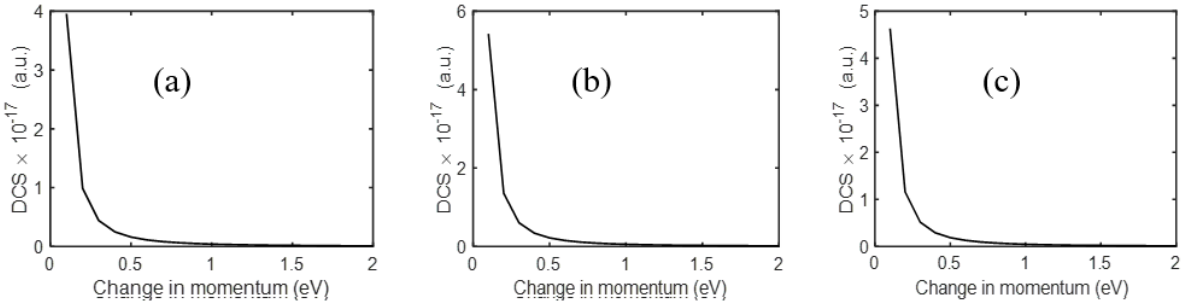

Figure 2: Dcs with change in momentum (a) linear, (b) elliptical, (c) circular of zero order bessel fucntion

Figures 3(a)–3(c) illustrate the variation of the DCS with photon energy. Across all polarization cases, the general trend shows that the DCS initially decreases as the photon energy increases, then remains constant over a certain range, and subsequently rises again with further increases in photon energy. The constant DCS region observed in Figure 3 corresponds to the equilibrium condition where the electrostatic interaction energy between the particles is equal to their rest energy. This plateau occurs within a specific range of the laser photon field. Once the photon energy increases beyond this range, the equilibrium is disrupted, and the DCS exhibits an exponential growth, indicating an increase in the repulsive force between the particles, which in turn leads to a greater separation of the charged particles. This behavior is particularly noticeable in the visible region, where the laser photon field produces a higher DCS compared to the infrared (IR) region, which shows lower DCS values but with unique and interesting electron–atom interaction characteristics under laser fields. When comparing the three polarization types, the DCS for elliptical polarization is consistently higher than that for circular polarization, while circular polarization yields higher DCS values than linear polarization.

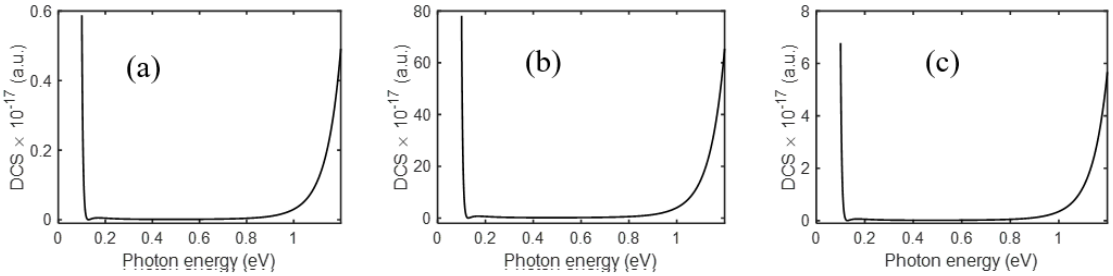

Figure 3: Dcs with photon enenrgy (a) linear, (b) elliptical, (c) circular of zero order bessel fucntion

Figure 4 depicts the variation of the DCS with the separation distance between the projectile and the target. In all polarization cases, the DCS for elliptical polarization is the highest, followed by circular polarization, with linear polarization producing the lowest values. For all three polarization types, an equilibrium position is observed at a separation distance below 1.6 (in the given units). This equilibrium corresponds to the condition where the electrostatic interaction energy equals the rest energy of the particles. Beyond this distance, the influence of the target's field becomes dominant over other effects at a fixed laser photon energy, momentum transfer, and scattering angle. Below the 1.6 separation threshold, variations in these other parameters have negligible impact on the electron–atom interaction. However, beyond this threshold distance, all parameters particularly the electromagnetic field interactions between charged particles play a significant role in determining the DCS behavior. Additionally, for validation, comparison with previous results (Kurmi et al., 2025) shows that the behavior of the DCS with respect to separation distance exhibits a similar trend.

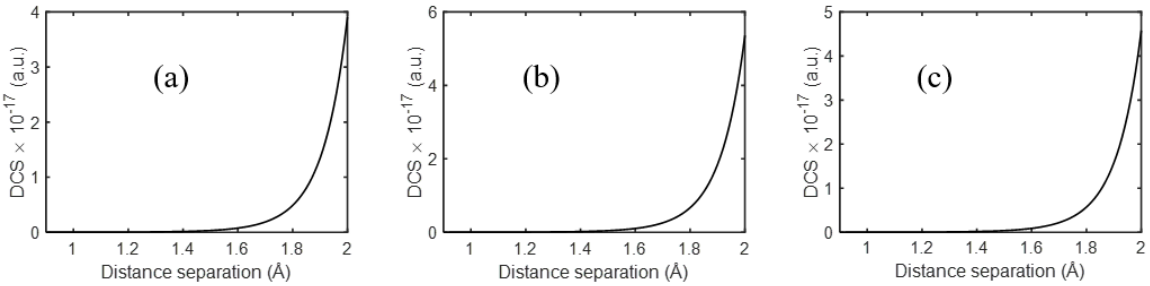

Figure 4: Dcs with distance sepration (a) linear, (b) elliptical, (c) circular of zero order bessel fucntion

DCS for first order Bessel function

Equation (16) was evaluated, and the resulting variation of DCS with scattering angle is presented in Figure 5. The results indicate that the DCS for linear polarization is the lowest, followed by circular polarization, while elliptical polarization yields the highest values. This ordering is consistent with the behavior observed for the zero-order Bessel function case. When comparing magnitudes, the DCS obtained using the first-order Bessel function is found to be lower than that from the zero-order Bessel function. For this reason, most researchers prefer to calculate or analyze the DCS using zero-order or lower-order Bessel functions, as higher-order Bessel functions significantly reduce the DCS magnitude. Such reductions not only make experimental measurement more challenging but also decrease precision in the results.

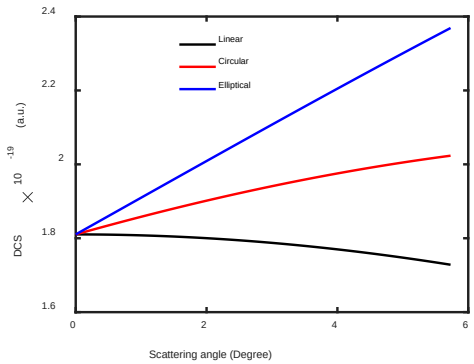

Figure 5: dcs with scattering anlge of first order bessel fucntion

Figure 6 presents the variation of the DCS with momentum transfer for the first-order Bessel function. In all polarization cases, the DCS increases with momentum change up to approximately 1 eV. Beyond this point, it decreases, reaching a minimum near 2.5 eV, after which it rises sharply. This trend is distinct from the zero-order Bessel function, where such a pattern was not observed. Additionally, the magnitude of the DCS for the zero-order case is consistently higher than that of the corresponding first-order case for the same polarization type. The initial gradual increase in DCS with momentum transfer suggests that the field is less dominant in this region. Around 1 eV, a slight resonance effect occurs due to the influence of the laser field, followed by a decline toward the minimum at about 2.5 eV. Beyond this point, another resonance emerges with a higher amplitude, leading to a steady increase in DCS. Since the resonance field amplitude is directly linked to the transition matrix, and the transition matrix is directly proportional to the DCS, these resonances significantly affect the observed scattering behavior.

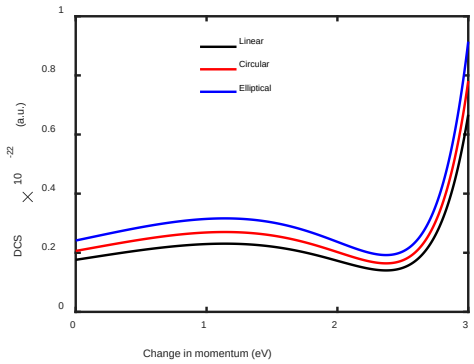

Figure 6: Dcs with change in momentum of first order bessel fucntion

Figure 7 illustrates the variation of the DCS with photon energy for the first-order Bessel function. The general trend is similar to that observed for the zero-order Bessel function; however, the overall magnitude of the DCS in the first-order case is lower. When comparing polarization types for the same order (first order), the DCS for elliptical polarization is consistently the highest, followed by circular polarization, with linear polarization producing the lowest values. This ordering reflects the broader interaction region associated with elliptical polarization and the more confined oscillation patterns of circular and linear polarizations.

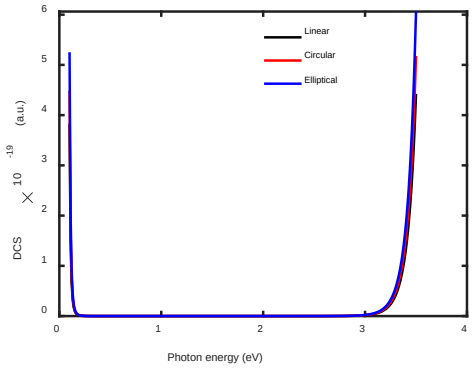

Figure 7: dcs with photon energy of first order bessel fucntion

Figure 8 shows the variation of the DCS with separation distance for the first-order Bessel function. The overall behavior is similar to that of the zero-order case, but with a lower DCS magnitude. A key difference is that, in this case, an equilibrium position is not observed beyond a separation distance of 1.4 Å. In the zero-order case, equilibrium was observed below 1.6 Å, whereas for the first-order case, even within 1.4 Å, such equilibrium was not detected. This indicates that for higher-order Bessel functions, the possibility of achieving equilibrium at separations greater than 1.4 Å does not exist.

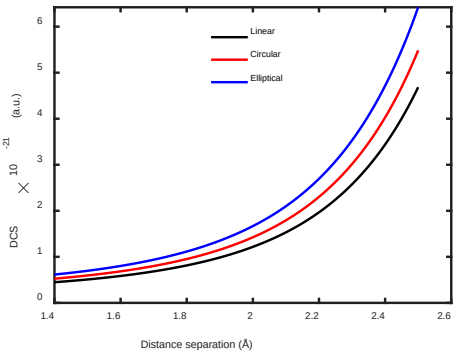

Figure 8: dcs with distance sperartion of first order bessel fucntion

Conclsuion

In general, the study demonstrates that the differential cross-section (DCS) is strongly influenced by polarization type, Bessel function order, and interaction parameters. Elliptical polarization consistently produces the highest DCS values, followed by circular and linear, due to differences in interaction coverage. Zero-order Bessel functions yield greater DCS magnitudes and more evident equilibrium regions than first-order functions. Variations in photon energy, momentum transfer, and separation distance reveal distinct regimes, with equilibrium occurring when electrostatic interaction energy equals particle rest energy. Resonance effects play a key role in shaping DCS behavior, highlighting the complex interplay between field characteristics and particle interactions.

References

Durak, S. (2016). Laser field effect on the nonlinear optical properties of quantum dots. (Doctoral dissertation, Dokuz Eylül University Graduate School of Natural and Applied Sciences).

Durak, S., & Sakiroglu, S. (2023). Theoretical investigation of laser field effect on nonlinear optical properties of quantum dots. Physica B: Condensed Matter, 650, 414575.

Kurmi, R. P., Yadav, K., Shrestha, A., & Dhobi, S. H. (2025). Laser assist quantum dot scattering with Gaussian potential. *Physics Open*, *23*, 100267.

Bohora, R., Yadav, K., & Dhobi, S. H. (2025). Differential Cross-Sections and Energy Shifts in Electron-Atom Scattering Under Linearly Polarized Laser Fields. *Journal of Optics and Photonics Research*, *2*(2), 86-92.

Dhobi, S. H., Yadav, K., Gupta, S. P., Nakarmi, J. J., & Jha, A. K. (2025). Non-monochromatic laser assist scattering in thermal environment. *Journal of the Nigerian Society of Physical Sciences*, 2345-2345.

Shrestha, C., Dhobi, S. H., & Shrestha, N. B. (2024). Strong-field nondipole approximation in laser-assisted thermal electron scattering. *Insight Physics*, *7*(1), 641.

Shrestha, N. B., Gupta, S. P., Poudel, Y., Yadav, K., Dhobi, S. H., & Nakarmi, J. J. (2023). Laser Assist Scattering in Lennard-Jones Potential. *Hadronic Journal*, *46*(4).

LaGattuta, K. J. (1994). Laser-assisted scattering from a one-dimensional δ-function potential: An exact solution. *Physical Review A*, *49*(3), 1745.

Wallbank, B., & Holmes, J. K. (1993). Laser-assisted elastic electron-atom collisions. *Physical Review A*, *48*(4), R2515.

Francken, P., & Joachain, C. J. (1990). Theoretical study of electron–atom collisions in intense laser fields. *Journal of the Optical Society of America B*, *7*(4), 554-563.

Kulander, K. C., Cooper, J., & Schafer, K. J. (1995). Laser-assisted inelastic rescattering during above-threshold ionization. *Physical Review A*, *51*(1), 561.

Anis, F., Roudnev, V., Cabrera-Trujillo, R., & Esry, B. D. (2006). Laser-assisted charge transfer in He 2++ H collisions. *Physical Review A—Atomic, Molecular, and Optical Physics*, *73*(4), 043414.

MiloŠević, D. B., Bauer, D., & Becker, W. (2006). Quantum-orbit theory of high-order atomic processes in intense laser fields. *Journal of Modern Optics*, *53*(1-2), 125-134.

Di Piazza, A., Müller, C., Hatsagortsyan, K. Z., & Keitel, C. H. (2012). Extremely high-intensity laser interactions with fundamental<? format?> quantum systems. *Reviews of Modern Physics*, *84*(3), 1177-1228.

Daniele, R., & Ferrante, G. (1981). Particle scattering in the presence of a strong multimode laser field. *Journal of Physics B: Atomic and Molecular Physics*, *14*(20), L635.

Yudin, G. L., & Ivanov, M. Y. (2001). Physics of correlated double ionization of atoms in intense laser fields: Quasistatic tunneling limit. *Physical Review A*, *63*(3), 033404.

Bucksbaum, P. H., Bashkansky, M., & McIlrath, T. J. (1987). Scattering of electrons by intense coherent light. *Physical review letters*, *58*(4), 349.

Metev, S. M., & Veiko, V. P. (2013). *Laser-assisted microtechnology* (Vol. 19). Springer Science & Business Media.

Liu, P., Wang, Q., & Li, X. (2009). Studies on CdSe/L-cysteine quantum dots synthesized in aqueous solution for biological labeling. Journal of Physical Chemistry C, 113(18), 7670–7676. doi:10.1021/jp901292q.

Kim, B.N. (2022).Angular Distribution of Electron-Helium Scattering in the Presence of A 1.17 eV Laser Field, Theses and Dissertations--Physics and Astronomy. 95.

Agrwal, B.K. & Prakash, Hari Quantum Mechanics Prentice Hall og India pvt. Ltd., New Delhi-110001, 2002

Maurer, J., and Keller, U. (2021). Ionization in intense laser fields beyond the electric dipole approximation: concepts, methods, achievements and future directions. Journal of Physics B: Atomic, Molecular and Optical Physics, 54(9)

Kroll, N.M. and Watson, K.M. (1973). Charged-particle scattering in the presence of a strong electromagnetic wave. Physical Review A, 8: 804–809.

Kavazović, K., Čerkić, A., & Milošević, D. B. (2021). Electron-molecule scattering in a bichromatic elliptically polarised laser field: Plateau structures and two-centre interference minima. *Molecular Physics*, *119*(14), e1948123